

Synthesis, structural characterisation and thermal decomposition of $[\{\text{Pt}(\text{dppf})(2\text{-SPy})\}\{\text{BF}_4\}](\text{dppf} = 1,1'\text{-bis(diphenylphosferrocene and 2-SPy} = 2\text{-mercaptopyridine)})$ – a source for a Fe–Pt containing alloy

V.D. de Castro^a, Geraldo M. de Lima^{a,*}, Arilza O. Porto^{a,*}, Helmuth G.L. Siebald^a, José D. de Souza Filho^a, J.D. Ardisson^b, José D. Ayala^a, Gabriella Bombieri^c

^a Departamento de Química, Universidade Federal de Minas Gerais – UFMG, Avenida Antonio Carlos 6627, Belo Horizonte MG 31270-901, Brazil

^b CDTN, Belo Horizonte MG 31270-901, Brazil

^c Istituto di Chimica Farmaceutica della Università di Milano, Milano, Italy

Received 28 May 2003; accepted 8 September 2003

Abstract

The reaction of 2-PySK with $[\text{Pt}(\text{dppf})\text{Cl}_2]$ [dppf = 1,1'-bis(diphenylphosferrocene and 2-PyS = 2-mercaptopyridine] produced $\text{Pt}(\text{dppf})(2\text{-SPy})_2$ (**1**) and its subsequent reaction with $\text{SnBu}_2(\text{BF}_4)_2$ or $\text{SnBu}_3(\text{BF}_4)$ yielded $[\{\text{Pt}(\text{dppf})(2\text{-SPy})\}\{\text{BF}_4\}]$ (**2**). Compounds **1** and **2** were fully characterised by multinuclear NMR [^1H , $^{13}\text{C}\{^1\text{H}\}$, $^{31}\text{P}\{^1\text{H}\}$ and $^{195}\text{Pt}\{^1\text{H}\}$] and ^{57}Fe Mössbauer spectroscopies. In addition the structure of **2** was determined by X-ray crystallographic studies, which can be summarised as follows: monoclinic $P2_1/c$, $a = 9.9291(9)$ Å, $b = 22.270(4)$ Å, $c = 16.919(2)$ Å, $\gamma = 103.6(9)^\circ$, $V = 3636.2(8)$ Å³ and $Z = 4$. Finally, a thermal decomposition study was carried out with **2** in three different atmosphere: oxygen, nitrogen or hydrogen. The residues were characterised by X-ray powder diffraction (XRD), X-ray electron probe microanalysis (EPMA), scanning electron microscopy (SEM) and ^{57}Fe Mössbauer spectroscopy. The results have shown the formation of a disordered $\text{Pt}_{1-x}\text{Fe}_x$ based alloy when the pyrolysis process was performed in H_2 , simultaneously with small amount of Fe(II) and Fe(III) phosphides. Furthermore, in oxygen and nitrogen the thermal decomposition of **2** produced metallic agglomerates of Pt dispersed in a combination of Fe(II) and Fe(III) phosphates in O_2 , and an intricate mixture of sulphides and phosphides in N_2 .

© 2003 Elsevier Ltd. All rights reserved.

Keywords: Pyrolysis; Organometallic compounds; Iron–platinum compounds

1. Introduction

The compound $[\text{Fe}(\eta^5\text{-C}_5\text{H}_4\text{PPh}_2)_2]$, dppf, still plays an important role in organometallic chemistry [1]. The coordination versatility of this metalloligand is highly remarkable. Actually, the various coordinating modes of dppf just reflect its ability to change conformation in order to match the steric demands of the surrounding molecular environment. However, in most examples it is η^2 bonded to metal centres. So far more than 250 structures determined by X-ray crystallography, con-

taining the dppf fragment, have been deposited at CCDC (version 5.24 of April 2003).

The considerable research attention granted to dppf relates to: (i) the various coordination modes towards metallic anions [2], (ii) the catalytic activity of the complexes [3] and (iii) the chemotherapeutic potential for cancer treatment of some derivatives [4].

Our research interest towards dppf concerns the preparation of well characterised Pt(II) [5], Ru(II), and its Sn(II)-containing heterometallic derivatives in order to obtain oxides and Fe/Pt/Sn or Fe/Ru/Sn containing alloys. For that, thermal decomposition of single source organometallic precursors has received special attention from us in the last two years [6]. Heterometallic

* Corresponding authors. Tel.: +553134995744; fax: +553134995720.
E-mail address: gmlima@dedalus.lcc.ufmg.br (G.M. de Lima).

derivatives of dppf seems to be attractive since it possesses different metallic species close enough to interact and produce synergetic effects which can result in interesting properties. Therefore, this work reports the thermal decomposition of $[\{Pt(dppf)(SPy)\}\{BF_4\}]$ (**2**) carried out in oxygen, nitrogen and hydrogen. The residues were studied by X-ray powder diffraction (XRD), scanning electron microscopy (SEM), X-ray electron probe microanalysis (EPMA) and ^{57}Fe Mössbauer spectroscopy.

2. Experimental

2.1. Synthesis and characterisation of metal complexes

The synthetic work was conducted in an atmosphere of dry N_2 . All solvents were treated by the appropriate method in order to remove moisture and oxygen, prior to use. All chemicals unless stated were obtained from Aldrich or Strem Co. NMR spectra were recorded in $CDCl_3$, at 400 MHz, 1H , 100.62 MHz; $^{13}C\{^1H\}$, 50.29 MHz; $^{31}P\{^1H\}$, 161.92 MHz; $^{195}Pt\{^1H\}$, 86.00 MHz using a Bruker DPX-400 spectrometer equipped with an 89 mm wide-bore magnet. ^{13}C and 1H shifts are reported relative to $SiMe_4$, ^{31}P to H_3PO_4 and ^{195}Pt to K_2PtCl_4 . Carbon and hydrogen elemental analyses were performed on a Perkin–Elmer PE-2400 CHN-analyses using tin sample-tubes. The X-ray diffraction data were collected using a Enraf Nonius FR590 with SMART CCD area detector and graphite–graphite-monochromated $Mo K\alpha$.

2.2. Synthesis of $Pt(dppf)(2-SPy)_2$ (**1**)

To a Schlenk-flask containing a suspension of 0.88 g (5.90 mmol) of 2-PySK and 20 ml of thf, was slowly added a thf solution of $[Pt(dppf)Cl_2]$, 2.42 g (2.95 mmol in 15 ml). Within 4 h of stirring the thf was removed in vacuum and CH_2Cl_2 (30 ml) was added in order to extract the product, originating an orange solution and KCl which was separated by filtration. A yellow solid was obtained after removing the solvent and re-crystallisation in CH_2Cl_2 /toluene (1:1, 30 ml). Yield based in $[Pt(dppf)Cl_2]$: 70% (2.00 g, 2.07 mmol). Mp 180(d) °C. 1H NMR δ 6.2–7.5(m) (Py and Ph), 4.4(s) and 4.2(s) (Cp); $^{13}C\{^1H\}$ NMR δ 168, 147, 137, 125, 115 (Py), δ 134–127 (Ph and Cp); $^{31}P\{^1H\}$ δ 16.87 $^1J(^{31}P-^{195}Pt) = 3139$ Hz; $^{195}Pt\{^1H\}$ δ -4684 $^1J(^{31}P-^{195}Pt) = 3195$ Hz. Elemental analysis for $C_{44}H_{38}FeP_2PtN_2S_2$, found (calc): C, 57.41(58.35); H, 3.99(4.01); N, 2.99(3.09)%.

2.3. Synthesis of $[\{Fe(\eta^5-C_5H_4PPh_2)_2Pt(SP_y)\}\{BF_4\}]$ (**2**)

To a solution of $AgBF_4$, 42 mg (0.22 mmol) in thf (20 ml), was added 70 mg (0.22 mmol) of $SnBu_3Cl$ in thf.

The clear solution remained stirring for 30 min in dark. The $AgCl$ formed was filtered off by cannula and the solution transferred to another Schlenk-flask containing 210 mg (0.22 mmol) of $Pt(dppf)(2-SPy)_2$ in thf (20 ml). After 15 h of stirring the solvent was removed and the residue was washed with *n*-hexane, extracting $SnBu_3-SPy$. The resultant golden-yellow solid was re-crystallised in toluene (30 ml) affording X-ray quality crystals. Yield 69% (144 mg, 0.150 mmol). Mp 215(d) °C. 1H NMR δ 7.9–6.6 (m) (Py and Ph), 4.9(s) and 4.4(s) (Cp); $^{13}C\{^1H\}$ NMR δ 166, 145, 136, 125, 119 (Py), δ 134–128 (Ph and Cp); $^{31}P\{^1H\}$ δ 17.27 $^1J(^{31}P-^{195}Pt) = 3162$ Hz and δ 11.56 $^1J(^{31}P-^{195}Pt) = 3609$ Hz; $^{195}Pt\{^1H\}$ δ -3500. Elemental analysis for $C_{39}H_{32}BF_4FeP_2PtS$, found(calc): C, 49.78(49.49); H, 2.81(2.78); N, 1.39(1.38)%. The same product was obtained using $SnBu_2Cl_2$ (50 mg, 0.16 mmol).

2.4. X-ray structure determination of **2**

The structure was solved by direct methods with SIR-92 [7] and the refinements were carried out using SHELXL 97 [8], minimising on the weighted *R* factor wR_2 . Further details are given in Table 1. All non-H atoms are anisotropic. The ORTEP drawing shows the non-H atoms as 50% thermal vibration ellipsoids. The crystals were obtained by slow evaporation of a toluene solution of **2**. The BF_4^- group showed to be very disordered.

Table 1
Crystal data and structure refinement for **2**

	2
Empirical formula	$C_{39}H_{32}BF_4FeP_2PtS$
Formula weight	946.41
Temperature (K)	263(2)
Wavelength	0.71073
Crystal system	monoclinic
Space group	$P2_1/c$
Unit cell dimensions	
<i>a</i> (Å)	9.9291(9)
<i>b</i> (Å)	22.270(4)
γ (°)	103.605(9)
<i>c</i> (Å)	16.919(2)
Volume (Å ³)	3636.2(8)
Calculated density (g cm ⁻³)	2.298
<i>Z</i>	4
Absorption coefficient	4.438
<i>F</i> (000)	1856
Crystal size (mm)	0.45 × 0.25 × 0.08
Theta range for data collection	2.48–28.54
Limiting indices	$h = 0-13; k = -29-0;$ $l = -22-22$
Reflections collected/unique	9260/6317
Refinement method	Full-matrix least-squares on F^2
Final <i>R</i> indices [$I > 2\sigma(I)$]	$R_1 = 0.032, wR_2 = 0.066$
<i>R</i> indices (all data)	$R_{1=0.078}, wR_2 = 0.076$
CCDC reference	192715

2.5. Thermal analysis of **2**

In order to determine the range of temperature of degradation of **2**, thermogravimetric analysis (TG) with simultaneous differential thermal analysis (DTA) experiments were performed in a TA Instruments SDT 2960 with a heating rate of 5 °C/min until 900 °C in oxygen.

2.6. Pyrolysis of **2**, chemical, structural and morphological characterisation of the residue

Thermal decomposition of **2** was carried out in a tube furnace in N₂, O₂ and H₂, using a heating rate of 5 °C/min until a final temperature of 900 °C employing a gas flux of 100 ml/min. The decomposed products were characterised by XRD, SEM, ⁵⁷Fe Mössbauer spectroscopy and EPMA.

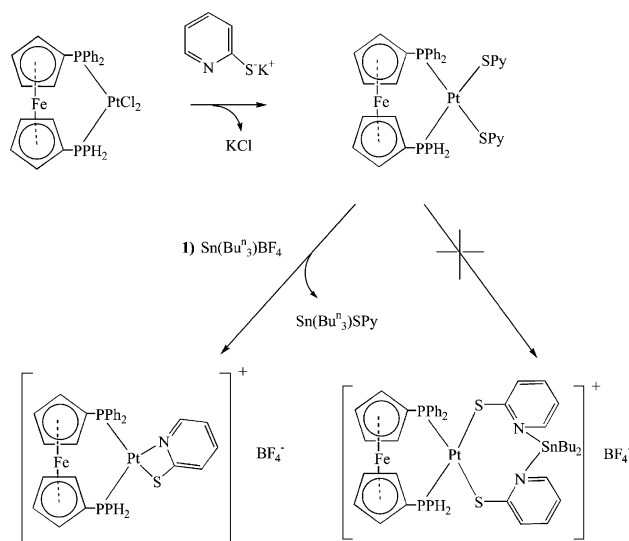
X-ray powder diffraction was executed in a Rigaku Geigerflex using a Cu K α radiation ($\lambda = 1.54178$ Å). A scan rate of 4°/min in the 2θ range from 4° to 100° was used. In those samples containing platinum its main diffraction line at 39.76° (111) was used as internal standard for angle calibration.

The scanning electron micrographs was recorded in a JEOL JSM-840A equipment and the electron probe X-ray microanalysis were carried out in a JXA 89000 RL wavelength dispersive/energy dispersive combined microanalyser. For the SEM images and X-ray microanalysis the samples were recovered with a thin film of gold and carbon, respectively, deposited by sputtering.

⁵⁷Fe Mössbauer measurements were obtained in order to identify the Fe oxidation states and number of different sites in the decomposed materials by using a conventional apparatus with ⁵⁷Co as source of γ -radiation, kept at room temperature.

3. Results and discussion

Organometallic compounds are good candidates for single source precursors for thermal decomposition because they decompose at low temperature, producing metallic oxides, metallic particles or inorganic salts. Following our interest in this research area, we have attempted to prepare a Pt/Fe/Sn derivative, as described in Scheme 1, to be employed as an source for the trimetallic containing materials. Firstly, the reaction of [Pt(dppf)Cl₂] with 2-PySK produced the bimetallic derivative [Pt(dppf)(SPy)₂] (**1**) (see Scheme 1) that was used as a S and N electron donor ligand towards another metal centre. Organotin(IV) Lewis acid were chosen due to the great Sn–N affinity observed in other complexes [9]. However, instead of a



Scheme 1. Pathway of the preparation of compound **1**.

simple coordination reaction, it was observed an exchange of 2-PyS[−] ligand between Pt(II) and Sn(IV) atoms.

Similar interchange was also detected when the reaction of [SnPh₃SPy] with [Pt(PPh₃)₂Cl₂] was performed in order to obtain a bimetallic complex where Pt(II) was coordinated through the S donor centre. However, two separated compounds SnPh₃Cl and [Pt(PPh₃)₂(SPy)₂] [10] were isolated and identified.

Compounds **1** and **2** are air and moisture stable golden-yellow products, readily soluble in CH₂Cl₂ and toluene, and they showed satisfactory results of elemental analysis. NMR spectroscopic measurements were carried out using a CHCl₃/CDCl₃ solutions. For both compounds the ¹³C and ¹H NMR spectra exhibited the expected resonances for Cp, Ph and Py groups. Compound **1** displayed a single signal at δ 16.9 [$J(^{31}\text{P}-^{195}\text{Pt}) = 3139$ Hz] in the ³¹P NMR spectrum, and a peak at δ −4684 [$J(^{31}\text{P}-^{195}\text{Pt}) = 3195$ Hz] in the ¹⁹⁵Pt NMR spectrum. It possesses a smaller ³¹P–¹⁹⁵Pt coupling constant, 3195 Hz compared to the starting material [Pt(dppf)Cl₂], 3768 Hz. The latter is a consequence of the better π -acceptor character of S compared to Cl which causes a decrease in the Pt–P bond strength.

The ³¹P NMR spectrum of **2** revealed two signals at δ 17.3 [$J(^{31}\text{P}-^{195}\text{Pt}) = 3162$ Hz] and 11.6 [$J(^{31}\text{P}-^{195}\text{Pt}) = 3609$ Hz]. Moreover, it was detected a coupling constant between the two non-equivalent phosphorus at 17 Hz. The first set of chemical shifts and coupling constants are similar to the signals displayed by **1**. Therefore, it might be assigned to the P atom *trans* to S of the –SPy moiety and the remaining signal can be attributed the other P atom *trans* to N. A broad resonance centred at δ −3500 was detected in the ¹⁹⁵Pt NMR spectrum, resulting from a complicated coupling pattern of ¹⁹⁵Pt with the non-equivalent ³¹P nuclei.

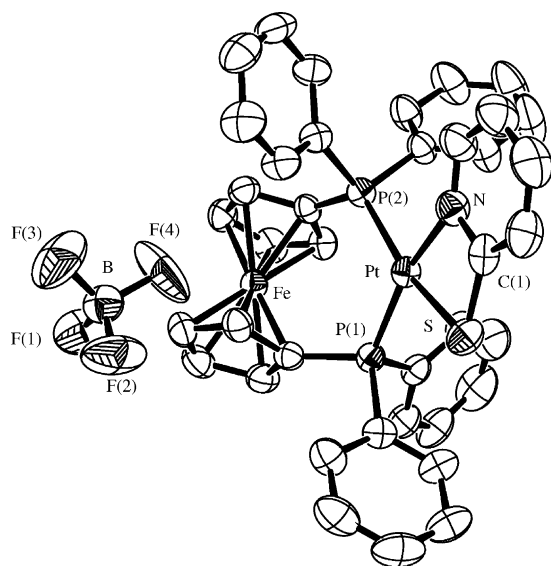


Fig. 1. Molecular structure of **2** determined by X-ray crystallography.

Table 2
Selected bond lengths (Å) and angles (°) for **2**

Bond lengths	
Pt–N	2.1160(4)
Pt–P(1)	2.2521(11)
Pt–P(2)	2.2910(11)
S–C(1)	1.7470(5)
Pt–S	2.3635(12)
Bond angles	
N–Pt–P(1)	164.07(14)
P(1)–Pt–P(2)	99.09(5)
P(1)–Pt–S	95.09(6)
S–C(1)–N	110.00(3)
N–Pt–P(2)	96.82(14)
N–Pt–S	69.00(14)
P(2)–Pt–S	165.81(6)

A single-crystal X-ray experiment confirmed the structure of **2** to be composed of Pt(dppf)(SPy)⁺ cations and BF₄[−] anions, with no direct contact between the two fragments, Fig. 1. The Pt(II) atom lies in the centre of a distorted square where it is bonded to both S {Pt–S, 2.3641(15) Å} and N {Pt–N, 2.113(5) Å} of the pyridyl group. These bond length and angles {N–Pt–S 69.00(14)°, P(1)–Pt–P(2) 99.09(5)°, S–C(1)–N 110.00(3)°} are very close to the ones observed for [{Pt(PPh₃)₂(SPy)}] {PF₆} [11] (Table 2).

The coordination position of the fluorine atoms in the BF₄[−] group was very disordered, similarly to other reported results [11].

3.1. Thermal analysis

Compound **2** displayed a highly exothermic decomposition process in a pseudo single step, which started at 300 °C and finished at 800 °C. The initial loss of weight

at 60 °C was subtracted from the curve in order to disregard the loss of solvent. In this step the complex loses 54.2% of the weight. After 400 °C, the material continues to decompose losing at the end, 800 °C, 47% of mass, leaving a final residue containing 7.2% of the initial amount, which suggests that an appreciable amount of material was lost to the gas phase.

3.2. X-ray electron probe microanalysis

The chemical composition of the residues was determined by EPMA in different regions of the samples in order to evaluate their level of homogeneity. The presence of carbon peaks in all residues is a consequence of the deposit of graphite at the sample's surface.

Two different regions were identified in the residues obtained in oxygen: a bright one, formed by agglomerates of metallic platinum (approximately 10 μm in size) dispersed in an amorphous media, dark region, constituted basically of P, Fe and O, Fig. 2. No sulphur was identified in this sample. A similar situation was revealed for the residue obtained in N₂, Fig. 3(b), however, the particles of platinum are much smaller than the previous one. Moreover, in this case it was noticed only a trace of oxygen, and the major components were Fe, P and S. The residue from decomposition of **2** in H₂ has not shown oxygen or sulphur, but only Pt, P and Fe, Fig. 3(c). The nature of the species formed could only be tentatively identified with the support of XRD and ⁵⁷Fe Mössbauer spectroscopies.

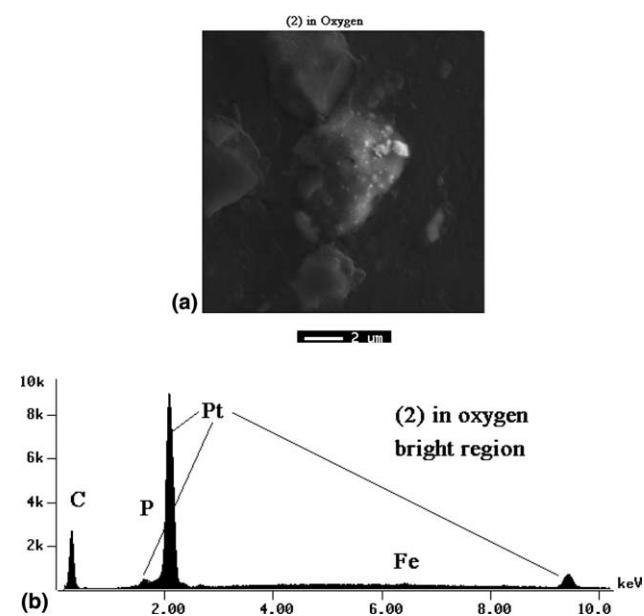


Fig. 2. The image and the dispersive energy X-ray microanalysis (EPMA) of **2** decomposed in O₂.

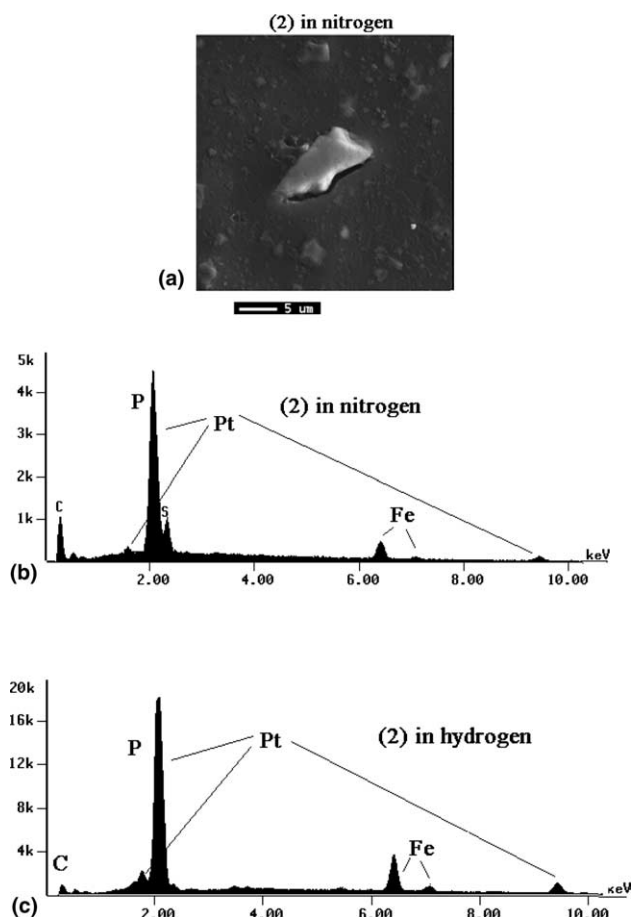


Fig. 3. (a) The image and the EPMA of **2** decomposed in N_2 (b) and H_2 (c).

3.3. X-ray powder diffraction

X-ray diffraction measurements were executed in order to identify the pyrolysis residues of **2**, Fig. 4. The diffractogram of the decomposed material in oxygen,

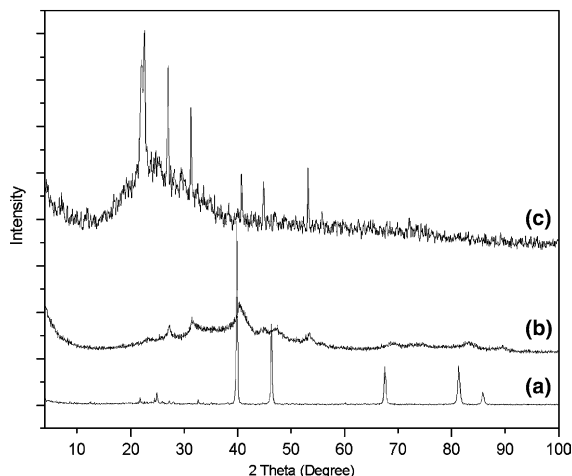


Fig. 4. XRD pattern of **2** decomposed in O_2 (a), N_2 (b) and H_2 (c).

Fig. 4(a) revealed lines at $2\theta = 39^\circ$, 46° , 67° and 81° ; corresponding, as indicated by the Miller index to the diffraction planes (1 1 1), (2 0 0), (2 2 0) and (3 1 1) to metallic platinum (Cubic, $Fm\bar{3}m$, $a = 3.923 \text{ \AA}$) [12]. The high intensity of the Pt diffraction lines suggests the production of large and well formed particles of platinum as observed in the electron backscattered image. The other diffraction lines can be clearly attributed to the formation of $FePO_4$ and $Fe_3(PO_4)_2$ [13] and it is in accordance to the EPMA and ^{57}Fe Mössbauer spectroscopic results.

Much more broader Pt diffraction lines (1 1 1), (2 0 0), (2 2 0) and (3 1 1) were revealed for the residue prepared in N_2 , in consequence of the lower crystallinity of the decomposed material. The much less intense lines at approximately $2\theta = 28^\circ$, 47° and 56° might be attributed to the cubic FeS [14a] {pyrite form – 06-0710} and those at $2\theta = 32^\circ$ and 53° which are also observed in the diffractogram of the sample decomposed in H_2 , can be associated to the orthorhombic FeP_4 [14b] {34-0996i}, Fig. 4(b). On the basis of the EPMA analysis there is no oxygen in the sample which frustrate the presence of phosphate anions. Therefore, it is reasonable to assume that Fe(II) and Fe(III) are in the form of sulphide and phosphide. The diffraction pattern of the product obtained in H_2 has shown lines, at $2\theta = 25^\circ$, 31° , 32° and 53° , corresponding to orthorhombic FeP_4 , as before, and the diffractions at $2\theta = 41^\circ$ and 46° , may be associated to the planes (1 0 0) and (2 0 0) of the Pt–Fe alloy (cubic – 29-0718). The intense line at $2\theta = 24^\circ$ is probably related to the alloy as well since other similar materials with different stoichiometry present diffraction lines at angles smaller than 30° [12].

3.4. ^{57}Fe Mössbauer experiments

The room temperature ^{57}Fe Mössbauer spectroscopy experiments supported the identification of iron compounds and its oxidation state, Fig. 5 and Table 3.

For the starting material, **2**, it was observed the presence of Fe(II) to which the parameters $\delta = 0.40(2) \text{ mm s}^{-1}$ and $\Delta = 2.25(3) \text{ mm s}^{-1}$ relates very well with the classical values reported for ferrocene, $[FeCp_2]$, $\delta = 0.44(2) \text{ mm s}^{-1}$ and $\Delta = 2.38(3) \text{ mm s}^{-1}$ and the dppf $\delta = 0.42(2) \text{ mm s}^{-1}$ and $\Delta = 2.30(3) \text{ mm s}^{-1}$ [15], Fig. 5(a). The ^{57}Fe Mössbauer spectrum of the residue prepared in O_2 , Fig. 5(b) displayed two signals with the corresponding parameters, $\delta = 0.30(2) \text{ mm s}^{-1}$, $\Delta = 0.44(3) \text{ mm s}^{-1}$ and $\delta = 0.37(2) \text{ mm s}^{-1}$, $\Delta = 0.98(3) \text{ mm s}^{-1}$ assigned to the presence of Fe(III), 63%, and Fe(II), 37%, respectively, that are in the form of phosphates [13]. Two sites of Fe(II), $\delta = 0.25(2) \text{ mm s}^{-1}$, $\Delta = 1.49(3) \text{ mm s}^{-1}$ (14%) and $\delta = 0.37(2) \text{ mm s}^{-1}$, $\Delta = 0.80(3) \text{ mm s}^{-1}$ (43%) and one site of Fe(III) $\delta = 0.29(2) \text{ mm s}^{-1}$, $\Delta = 0.23(3) \text{ mm s}^{-1}$ (43%) were

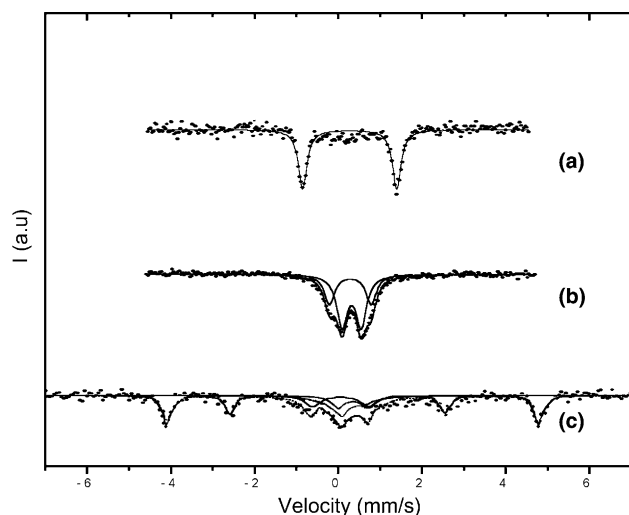


Fig. 5. ^{57}Fe Mössbauer spectra of **2** and the corresponding residues obtained in O_2 (a), N_2 (b), and H_2 (c).

found in the material obtained in N_2 , Fig. 5(c). The iron species are associated to the sulphide and phosphide, as attested by the other results. Finally, the sample obtained in H_2 presents signals related to Fe(II), $\delta = 0.36(2) \text{ mm s}^{-1}$, $\Delta = 0.83(3) \text{ mm s}^{-1}$ (12%), and Fe(III) with $\delta = 0.26(2) \text{ mm s}^{-1}$, $\Delta = 0.12(3) \text{ mm s}^{-1}$ (11%). These cations are in the form of orthorhombic phosphide FeP_4 as the XRD pointed out. The more remarkable is the sextet with $\delta = 0.26(2) \text{ mm s}^{-1}$, $\Delta = 0.19(3) \text{ mm s}^{-1}$ and a hyperfine field ($B_{\text{hf}} = 27 \text{ T}$ (77%)), which indicates some form of metallic iron, Fig. 5(e). It was attributed to a disordered $\text{Pt}_{1-x}\text{Fe}_x$ phase on the basis of the ^{57}Fe Mössbauer parameters of

Table 3
 ^{57}Fe Mössbauer parameters for the complex **2** and the residue of decomposition of **2** under O_2 (a), N_2 (b) and H_2 (d)

Sample	Fe oxidation state	IS (mm s^{-1})	QS (mm s^{-1})	Area (%)
2	Fe(II)	0.40	2.25	100
O_2	Fe(III)	0.30	0.44	63
	Fe(II)	0.37	0.98	37
N_2	Fe(III)	0.30	0.44	43
	Fe(II)	0.25	1.49	14
	Fe(II)	0.37	0.80	43
H_2	Fe	0.26	0.19	77
	Fe(III)	0.26	0.12	11
	Fe(II)	0.36	0.83	12

The experimental errors associated to IS and QS are 0.02, 0.03, respectively.

other Fe/Pt alloys [16] and the data of metallic iron $\delta = 0.29(2) \text{ mm s}^{-1}$, $\Delta = 0.14(3) \text{ mm s}^{-1}$ and $B_{\text{hf}} = 28 \text{ T}$. The experiments of ^{57}Fe Mössbauer have shown the formation of different sites of iron which can not be directly attributed to any particular compound without the help of other techniques. However, it is clear that a very different iron phase is formed in the sample decomposed in H_2 , that is very similar to the pattern exhibited for iron containing alloys. No further evidence was found for the formation of iron carbides, carbonates or oxides, at least as major products.

3.5. Scanning electron microscopy

The SEM images, Fig. 6, were obtained for each residue in order to investigate the level of homogeneity

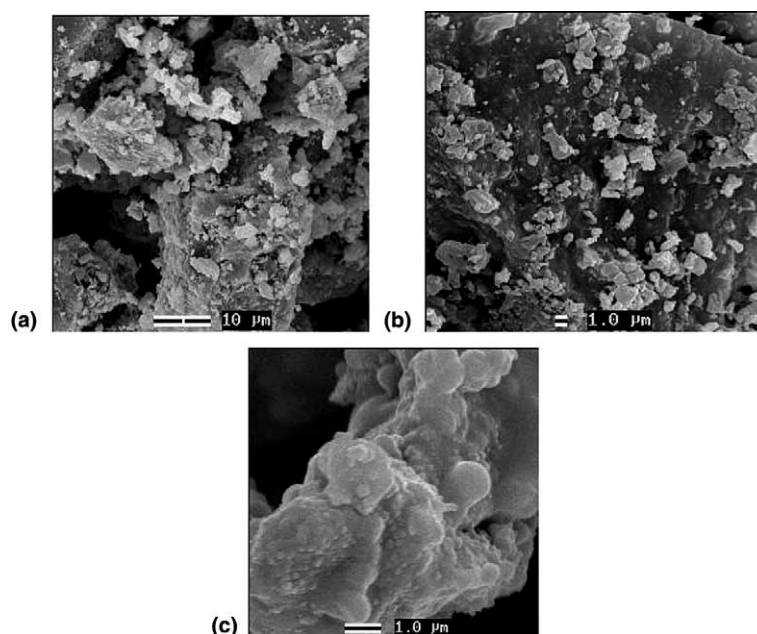


Fig. 6. Electron scanning micrographs of **2** decomposed in O_2 (a), N_2 (b) and H_2 (c).

and the presence of metallic agglomerates. No considerable difference is observed for the decomposed material in O₂, Fig. 6(a), or N₂, Fig. 6(b). It is obvious since the grains correspond to the presence of metallic platinum. The major difference consists in the nature of the dark and amorphous material that in the first case consists of a mixture of Fe(II) and Fe(III) phosphates and in the second product it is associated to a complex combination of Fe(II) and Fe(III) phosphides or sulphides. Also, the size of the particles obtained in oxygen vary from 40 to 70 μm whilst in nitrogen it is much smaller. In the case of **2** decomposed in H₂ a more compact and homogenous material was obtained and seems to be formed by very big grains (100–200 μm).

4. Conclusions

In this work the synthesis and structural characterisation of [$\{\text{Pt}(\text{dppf})(\text{SPy})\}\{\text{BF}_4\}$] (**2**) was described. The thermal behaviour of **2** was studied by simultaneous TG/DTA measurements. The preparation of products of decomposition of **2** in O₂, N₂ and H₂ was investigated and the obtained residue was fully characterised by XRD, SEM, EPMA and ⁵⁷Fe Mössbauer spectroscopy. The results have attested the formation of a disordered Pt_{1-x}Fe_x alloy when the pyrolysis process was performed in H₂. However, the procedure also produced Fe(II) and Fe(III) containing materials, as contaminants. The degradation product of **2** in O₂ and N₂ consisted of metallic platinum and again Fe(II) and Fe(III) species.

5. Supplementary data

Crystallographic data for the structural analysis of compound **1** have been deposited at the Cambridge Crystallographic Data Centre, 12 Union Road, Cambridge, CB2 1EZ, UK, and are available free of charge from the Director on request quoting the deposition number CCDC 192715 (fax: 44-1223-336033; e-mail: deposit@ccdc.cam.ac.uk or www: <http://www.ccdc.cam.ac.uk>).

Acknowledgements

We thank TWAS – Third World Academy of Science (Research Grant Agreement 00-229 RG/CHE/LA) and CNPq-Brazil for the financial support. The present work

was partially developed at the Laboratório de Microscopia Eletrônica e Microanálise (LMA) – Física, Química, Geologia-UFMG and CDTN-CNEN financed by FAPEMIG (Project CEX 1074/95).

References

- [1] G. Bandoli, A. Dolmella, *Coord. Chem. Rev.* 209 (2000) 161.
- [2] W.-Y. Yeh, Y.J. Cheng, M.Y. Chiang, *Organometallics* 16 (1997) 918.
- [3] K.S. Chan, T.S.A. Hor, in: A. Togni, T. Hayashi (Eds.), *Ferrocenes – Homogenous Catalysis, Organic Synthesis and Material Science*, VHC, Weinheim, 1995, p. 3.
- [4] M. Viotte, B. Gautheron, I. Nifantév, L.G. Kuz'mina, *Inorg. Chim. Acta* 253 (1996) 71.
- [5] G.M. de Lima, C.A.L. Filgueiras, M.T.S. Giotto, Y.P. Mascarenhas, *Transition Met. Chem.* 26 (1995) 380.
- [6] (a) A.G. Pereira, A.O. Porto, G.M. de Lima, G.G. Silva, H.G.L. Siebald, J.L. Neto, *Phys. Chem. Chem. Phys.* 4 (2002) 4528; (b) G.A.A. Costa, M.C. Silva, A.C.B. Silva, G.M. de Lima, R.M. Lago, M.T.C. Sansiviero, *Phys. Chem. Chem. Phys.* 2 (2000) 5708.
- [7] (a) G.M. Sheldrick, *SHELXL 5.0*, Siemens Analytical Instruments, Madison, WI, 1994; (b) A. Altomare, G. Cascarano, C. Giacovazzo, A. Guagliardi, *J. Appl. Cryst.* 26 (1993) 343.
- [8] (a) G.M. Sheldrick, *SHELXL 96*, University of Göttingen, Germany, 1996; (b) G.M. Sheldrick, *SHELXL 97*, Program for Refinement of Crystal Structures, University of Göttingen, Germany, 1997.
- [9] (a) I. Omae, *Organotin Chemistry*, Elsevier, Amsterdam, 1989; (b) G. Wilkinson, F.G.A. Stone, E.W. Abel (Eds.), *Comprehensive Organometallic Chemistry*, vol. 3, Pergamon Press, Oxford, 1982, p. 1043.
- [10] V.D. de Castro, G.M. de Lima, C.A.L. Filgueiras, M.T.P. Gambardella, N.L. Speziali, *Main Group Met. Chem.* 24 (2001) 761.
- [11] S. Wang, R.J. Staples, J.P. Fackler Jr., *Acta Crystallogr., Sect. C* 50 (1994) 889.
- [12] All the XRD data are related to JCPDS – ICDD – 1997.
- [13] (a) R. Jones, P.F. Kelley, C.P. Warrens, D.J. Willians, J.D. Wollins, *J. Chem. Soc., Chem. Commun.* (1986) 711, *J. Chem. Soc., Chem. Commun.* (1988) 1569; (b) O.L. Casagrande Jr., A.E. Gerbase, F.C. Stedile, F.O.V. da Cunha, L. Amaral, I.J.R. Baumvol, *Polyhedron* 16 (1997) 171.
- [14] (a) T. Douglas, D.P.E. Dickson, S. Betteridge, J. Charnock, E.D. Garner, S. Mann, *Science* 269 (1995) 54; (b) M. Sugitani, N. Kinomura, M. Koizumi, S. Kume, *J. Solid State Chem.* 26 (1978) 195.
- [15] (a) I.R. Butler, W.R. Cullen, J. Trotter, *Organometallics* 4 (1985) 972; (b) G.M. de Lima, C.A.L. Filgueiras, A. Abras, *Hyperfine Interactions* 83 (1994) 183.
- [16] (a) T. Goto, H. Utzugi, A. Kashiwakura, *J. Magn. Magn. Mat.* 104–107 (1992) 2051; (b) U. Gonser, S. Nasu, W. Kappes, *J. Magn. Magn. Mat.* 10 (1979) 244; (c) J.G. Na, *J. Mat. Sci. Lett.* 19 (2000) 1171.